J Inf Process Syst, Vol.13, No.4, pp.677~688, August 2017
https://doi.org/10.3745/JIPS.02.0064

ISSN 1976-913X (Print)
ISSN 2092-805X (Electronic)

JOURNAL OF INFORMATION PROCESSING SYSTEMS JIPS

Time-Delay and Amplitude Modified BP Imaging Algorithm of Multiple Targets for UWB Through-the-Wall Radar Imaging

Huamei Zhang*, Dongdong Li*, Jinlong Zhao*, and Haitao Wang*

Abstract

In order to solve the undetected probability of multiple targets in ultra-wideband (UWB) through-the-wall radar imaging (TWRI), a time-delay and amplitude modified back projection (BP) algorithm is proposed. The refraction point is found by Fermat's principle in the presence of a wall, and the time-delay is correctly compensated. On this basis, transmission loss of the electromagnetic wave, the absorption loss of the refraction wave, and the diffusion loss of the spherical wave are analyzed in detail. Amplitude compensation is deduced and tested on a model with a single-layer wall. The simulating results by finite difference time domain (FDTD) show that it is effective in increasing the scattering intensity of the targets behind the wall. Compensation for the diffusion loss in the spherical wave also plays a main role. Additionally, the two-layer wall model is simulated. Then, the calculating time and the imaging quality are compared between a single-layer wall model and a two-layer wall model. The results illustrate the performance of the time-delay and amplitude-modified BP algorithm with multiple targets and multiple-layer walls of UWB TWRI.

Keywords

Amplitude Modified Back Projection, Time Delay, Through-the-Wall Imaging, Ultra-Wideband

1. Introduction

Through-the-wall radar imaging (TWRI) is a form of nondestructive detection and can precisely and quickly locate targets behind obstacles. TWRI has played an important role in military applications, the fight against terrorism, and search and rescue efforts after earthquakes. Thus, it has become more attractive in many civilian and military applications [1-3].

An ultra-wideband (UWB) signal is a short duration pulse in the time domain and has a very wide bandwidth in the frequency domain. UWB signals work at a frequency that is low enough to penetrate walls, and their bandwidth is wide enough to clearly identify targets behind walls. UWB radar systems satisfy the requirements for both low frequency and large bandwidth. The imaging method based on UWB radar systems is clearly described in many studies [4-6]. Numerous efforts have provided high-quality focused applications for walls consisting of wood, glass, plastic, drywall, brick, or concrete blocks and, in most of cases, walls that are multi-layered and non-homogeneous. Some results obtained

Manuscript received November 17, 2014; first revision October 13, 2015; accepted December 8, 2015.
Corresponding Author: Huamei Zhang (zhanghm@njupt.edu.cn)
* School of Electronic Science and Engineering, Nanjing University of Posts and Telecommunications, Nanjing, China (zhanghm@njupt.edu.cn, ({513052267, 395419675, 871209769}@qq.com)

images behind a multi-layered, non-homogeneous wall using an auto-focusing imaging algorithm [7]. The algorithm searches for the best time-delay focusing in the assumed range to approximately compensate for different propagation time-delays from anomalous propagations in the walls. Although the algorithm can implement high-quality target imaging with fine focusing degrees and minor target displacement, it can only address a single target behind the wall and is not suitable for multiple targets.

Ahmad et al. [8] placed two target images in the presence of a single uniform wall. She implemented multi-target imaging, but the target close to the radar antenna system absorbed a large amount of energy and the electromagnetic waves reflected from the other targets had a small magnitude. If the room is large and the energy emission is small, the target behind the wall may not be detected. For signal processing with multiple targets [9,10], cross-range resolution is enhanced, but this applies to a single, uniform wall. Urdiik et al. [11] used weak signal enhancement methods in combination with proper target detectors. He proposed six methods that have the ability to enhance a weak signal to improve the results of radar detection.

The back projection (BP) algorithm is a conventional delay-and-sum beam-forming algorithm and is known as the most used imaging algorithm in TWRI [2,12,13]. The BP algorithm can address point target imaging in a homogenous medium very well, but it is not suitable for a layered lossy medium. In the process of an electromagnetic wave going through a wall, the propagation speed will change, refraction will occur and the signal amplitude will attenuate. All of these factors will lead to defocused target images, displacing targets from their true positions, and possibly producing false targets. When multiple targets are behind a wall, the scattering intensity of the post-target is smaller than the scattering intensity of the pre-target, and the post-target might not be detected. In order to obtain a high-quality focused image in a layered lossy wall, it is necessary to modify the BP algorithm to correct the transmission effects and amplitude attenuation. A TAM-BP imaging algorithm is proposed in a ground penetrating radar (GPR) application [14]. But in that situation, the electromagnetic wave transmits from the air to the lossy medium (soil). However, in TWRI, the electromagnetic wave transmits the lossy medium (a single wall, sometimes multiple walls) to the air. The propagation medium is two layers in GPR and three or more layers in TWR. Thus, the TWR model is more complicated than the GPR model and requires more consideration.

In this paper, we propose a time-delay and amplitude modified BP imaging algorithm that compensates for the time delay and amplitude attenuation in a TWRI application.

This paper is organized as follows: in Section 2, we provide the processing procedure of the modified BP algorithm in detail. In Section 3, single-layer and two-layer wall models are simulated by FDTD, and the simulated results are obtained with the modified BP algorithm. Imaging time and compensation effects are also discussed in this section. Section 4 concludes this paper.

2. Time-Delay and Amplitude Modified BP Imaging Algorithm

The BP algorithm is a time domain algorithm and is characterized by a time delay, eliminating the influence of the Doppler shift and greatly simplifying the calculations. Because of the BP algorithm's high accuracy, it is effective for analysis of TWRI.

The BP algorithm originates from computer tomography technology. The imaging data comes from the receiving antenna array. In forward modeling, a set of electric field values, which serve as a function

of time, are obtained. Scattering echo data are obtained by the background subtraction method, which subtracts electric field values with targets and without targets. The scattering data are used in the BP algorithm, which is implemented as follows:

Step 1. Divide the whole region of interest into small surface areas or pixels.

Step 2. For each pixel, calculate the total flight time from transmitter to pixel and pixel to receiver.

Step 3. Record the corresponding received time bin amplitude for each pixel.

Step 4. Repeat Steps 2 and 3 for all receivers.

Step 5. Sum the recorded amplitudes on the spatial grid.

In free space, the back projected signal at pixel (*x*, *y*) in the room image plane is given by:

$$I(x,y)=\sum_{n} E\left(t(n)\right) \tag{1}$$

where, $t(n)=\dfrac{R_t(n)+R_r(n)}{c}$ is the total time for the transmitted signal to travel to pixel (*x*, *y*) and then travel back to receiver *n*; *c* is the speed of light in free space; $R_t(n)=\sqrt{(x-x_t)^2+(y-y_t)^2}$ is the distance between the transmitter antenna and pixel (*x*, *y*); and $R_r(n)=\sqrt{(x-x_r)^2+(y-y_r)^2}$ is the distance between pixel (*x*, *y*) and the receiver antenna. $E(t(n))$ is the sum of the signal amplitudes.

In the presence of a wall, the electromagnetic wave does not travel along a straight line any longer. Thus, when the refraction points are first found accurately, the transmitting path and the reflection coefficient can be determined.

Fig. 1 shows the geometry of the propagation path model. Mediums 1 and 3 are free space, and medium 2 is a wall whose permittivity, conductivity, and thickness are denoted as ε_w, σ_w, and d_w, respectively. In the simulation, the wall is a nonmagnetic medium whose permeability is μ_0. μ_0 is the permeability in free space. Because the relative permittivity is not equal to 1 and the conductivity is not equal to 0, the permittivity, wave impedance, and the wave number of the wall are complex numbers.

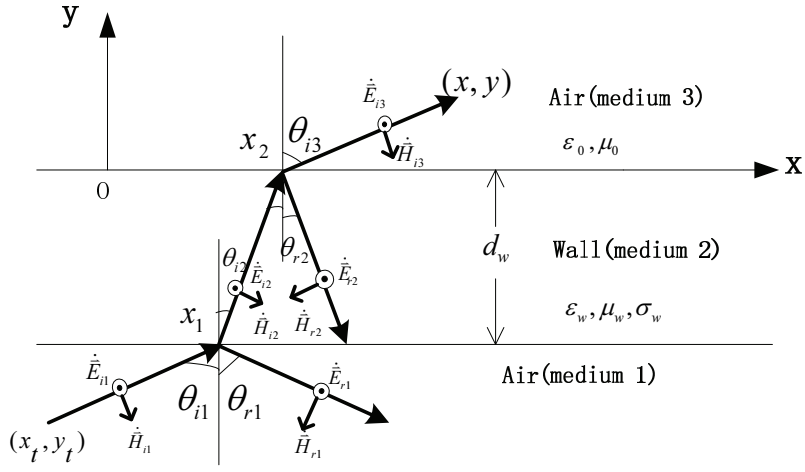

Fig. 1. Geometry depicting the effect of refraction on propagation.

We assumed that the transmitter antenna with coordinate (x_t, y_t) is located in medium 1 and that a point target with coordinate (x, y) is located in medium 3. When the electromagnetic wave transmits through the wall, refraction will occur at the interface between the wall and the air. The refraction point is $(x_1, -d_w)$, which is at the interface between medium 1 and medium 2, and $(x_2, 0)$, which is at the interface between medium 2 and medium 3.

First, the effect of conductivity on the refraction of the electromagnetic waves was considered. According to $\frac{\sigma_w}{\omega\varepsilon_w}$, the wall is a weak lossy medium. The speed of electromagnetic waves in the wall is approximated by $v = \frac{c}{\sqrt{\varepsilon_r}}$, where ε_r is the relative permittivity of the wall. The transmission time of electromagnetic waves from the transmitter antenna to the pixel was calculated as follows:

Propagation distance of the signal inside the wall: $l_1 = \sqrt{(x_1 - x_2)^2 + d_w^2}$

Propagation distance of the signal inside the free space: $l_2 = \sqrt{(x - x_2)^2 + y^2}$, $l_3 = \sqrt{(x_t - x_1)^2 + (y + d_w)^2}$

The total time for the signal to travel from the transmitter antenna to the pixel was:

$$t_{xyt}(n) = \frac{\sqrt{\varepsilon_r} l_1 + l_2 + l_3}{c} \tag{2}$$

We were able to find the precise refraction point according to four quadratic equations so that we could accurately calculate the total time. However, if the wall is not a single layer and consists of two or more layers, theoretically, the analytical solution can still be obtained, but the equations will be too numerous to calculate. According to Fermat's principle, the time is shortest if the electromagnetic waves travel along the actual path. In this paper, we adopted the searching method that took the shortest amount of time to find the refraction point. According to the location of the refraction points and antenna, propagation time t_{xyt} from the transmitter antenna to the pixel was calculated. Using the same method, t_{xyr} from the pixel to the receiver antenna was also calculated. As a result, the total time $t_{xyt} + t_{xyr}$ was obtained.

This resulted in the imaging function being:

$$I(x, y) = \sum_n E\left(t_{xyt} + t_{xyr}\right) \tag{3}$$

Thus, the time delay was well compensated. In this paper, amplitude modification is primarily discussed, and transmission loss, absorbing loss, and diffusion loss are analyzed in detail below.

Assume that the wave impedance of mediums 1, 2, and 3 is Z_{w1}, Z_{w2}, Z_{w3}, respectively, and $\theta_{i1} = \theta_{r1} = \theta_1$, $\theta_{i2} = \theta_{r2} = \theta_2$, and $\theta_{i3} = \theta_3$. The reflection coefficient Γ_{up} of the interface between mediums 2 and 3 and the reflection coefficient Γ_{down} of the interface between mediums 1 and 2 are calculated, respectively, as follows:

$$\Gamma_{up} = \frac{Z_{w_3}\cos\theta_2 - Z_{w_2}\cos\theta_3}{Z_{w_3}\cos\theta_2 + Z_{w2}\cos\theta_3} \tag{4}$$

$$\Gamma_{down}=\frac{\cos\theta_2 Z_{w_2}\left(\cos\theta_1 Z_{w3}-\cos\theta_3 Z_{w1}\right)+j\left(\cos\theta_1\cos\theta_3 Z_{w_2}^2-\cos^2\theta_2 Z_{w1}Z_{w3}\right)\tan\left(k_2 d_w\cos\theta_2\right)}{\cos\theta_2 Z_{w_2}\left(\cos\theta_1 Z_{w3}+\cos\theta_3 Z_{w1}\right)+j\left(\cos\theta_1\cos\theta_3 Z_{w_2}^2+\cos^2\theta_2 Z_{w1}Z_{w3}\right)\tan\left(k_2 d_w\cos\theta_2\right)} \tag{5}$$

where k_2 is the wave number of medium 2, which is the wall in this paper.

Because medium 1 and medium 3 are both free space, $Z_{w3}=Z_{w1}$ and $\theta_3=\theta_1$, Eqs. (4) and (5) can be simplified as:

$$\Gamma_{up}=\frac{Z_{w1}\cos\theta_2-Z_{w_2}\cos\theta_1}{Z_{w1}\cos\theta_2+Z_{w2}\cos\theta_1} \tag{6}$$

$$\Gamma_{down}=\frac{j\left(\cos^2\theta_1 Z_{w_2}^2-\cos^2\theta_2 Z_{w_1}^2\right)\tan k_2 d\cos\theta_2}{2\cos\theta_1\cos\theta_2 Z_{w_1}Z_{w_2}+j\left(\cos^2\theta_1 Z_{w_2}^2+\cos^2\theta_2 Z_{w_1}^2\right)\tan k_2 d\cos\theta_2} \tag{7}$$

According to Γ_{up} and Γ_{down}, the transmission loss is:

$$L_{trans}=\frac{(1+\Gamma_{down})(1+\Gamma_{up})}{e^{jk_2 d_w\cos\theta_2}+\Gamma_{up}e^{-jk_2 d_w\cos\theta_2}} \tag{8}$$

Moreover, the wall is always lossy, and the wavefront and constant amplitude surface is not the same when the electromagnetic wave has an oblique incidence from the free space to the wall. The amplitude of the refraction wave affected by the wall conductivity attenuates along the vertical wall direction. The absorbing loss is:

$$L_{absorb}=e^{-\xi y} \tag{9}$$

where ξ is the attenuation factor and the specific expression is:

$$\xi^2=\{(k_2^{'})^2-(k_2^{''})^2-k_1^2\sin^2\theta_1+\sqrt{(2k_2^{'}k_2^{''})^2+[(k_2^{'})^2-(k_2^{''})^2-k_1^2\sin^2\theta_1]^2}\}/2 \tag{10}$$

Where $k_1=\omega\sqrt{\mu_0\varepsilon_0}$ is the wave number of the free space, $k_2=k_2^{'}-jk_2^{''}=\omega\sqrt{\mu_w\varepsilon_w}=\omega\sqrt{\mu_0(\varepsilon_0\varepsilon_r+j\frac{\sigma}{\omega})}$.

If the wall is a weak lossy medium, $k_2^{'}=\omega\sqrt{\mu_w\varepsilon_w}=\omega\sqrt{\mu_0\varepsilon_0\varepsilon_r}$, $k_2^{''}=\frac{\sigma_w}{2}\sqrt{\frac{\mu_w}{\varepsilon_w}}=\frac{\sigma_w}{2}\sqrt{\frac{\mu_0}{\varepsilon_0\varepsilon_r}}$.

Otherwise, in the TWRI system, the targets are located in the near-field region of the antenna, and the diffusion loss of the spherical wave leads to amplitude attenuation with increasing propagation distance. We assumed that the transmission power of the transmitter antenna was P_t and that the reception power of the receiver antenna was P_r. Thus, the diffusion loss in the air is:

$$L_{air}=10\log\left(P_t/P_r\right)=32.4478+20\log f\left(MHz\right)+20\log r\left(km\right) \tag{11}$$

where f is the frequency of the electromagnetic waves and r is the distance between the transmitter antenna and the receiver antenna.

If all losses are considered at the same time, the compensation factor can be expressed as: $L_{\text{total}} = (L_{\text{air}} \cdot L_{\text{trans}} \cdot L_{\text{absorb}})^2$. Then, the amplitude compensation is applied to the conventional BP algorithm (i.e., a step is added between Step 4 and Step 5 for the amplitude compensation at every pixel).

3. Numerical Simulations

A general schematic of TWRI is shown in Fig. 2. The coordinate origin is located in the lower left corner of the model. The length of the wall was 2.4 m, and the thickness was 0.1 m. Because it is impossible to rigorously calculate the time-delay focus due to the non-homogeneity of each layer of the wall [7] and the fact that in most research the wall can be equivalent to a homogeneous one, we assumed the wall to have homogeneous conductivity and to be a homogenous concrete wall whose relative permittivity is $\varepsilon_r = 4.5$ and conductivity $\sigma_w = 0.03$. Because $\frac{\sigma_w}{\omega\varepsilon_w} = 0.06 \prec\prec 1$, we were able to use the results, as shown in Section 2. The antenna that transmitted and received signals moved parallel to the wall and synthesized a measurement aperture of L = 2.4 m. The antenna was located 0.04 m away from the wall, and the spatial sampling interval was 0.02 m. Two square metal bodies that were 0.1 m in length were located behind the wall, and the center coordinates of the metal bodies were (0.65 m, 1.05 m) and (1.65 m, 1.85 m).

The geometry of the TWRI was discretized with FDTD square cells that were 1cm in length. The time resolution was 16.7 ps. In the FDTD simulation, the transmitting signal was a 0.6 ns Gaussian pulse modulated by a 2-GHz sine wave. Its 3 dB bandwidth was 2.1 GHz, and the percentage bandwidth was 105%. The transmitting signal was a UWB signal. The waveform in the time domain and frequency domain are shown in Fig. 3.

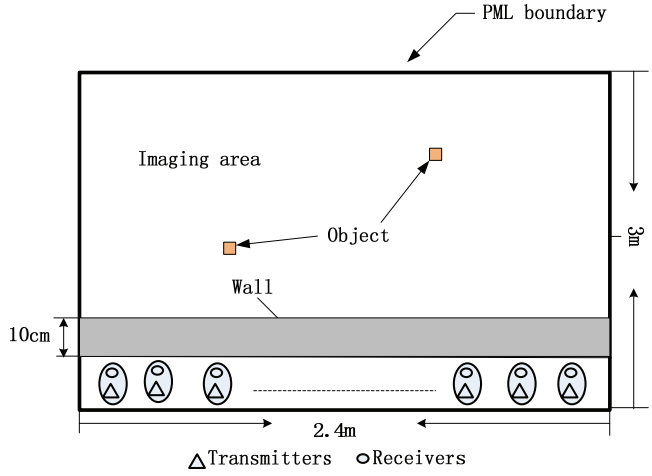

Fig. 2. Schematic of through-the-wall radar imaging.

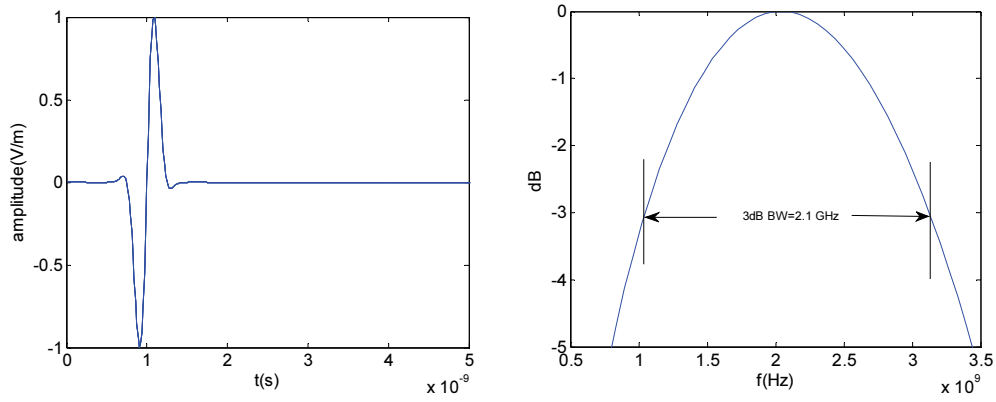

(a) (b)

Fig. 3. Time and frequency response of the UWB excitation pulse. (a) Waveform in the time domain and (b) waveform in the frequency domain.

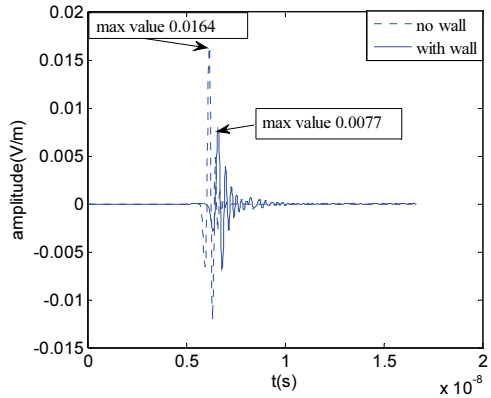

Fig. 4. The receiving signal of the 45th sampling location.

The waveform of the receiver data with and without the wall for the 45th sampling location is given in Fig. 4, which shows the amplitude attenuation and time delay when the signal travelled through the wall. Thus, time-delay compensation and amplitude modification is necessary when using the BP algorithm. The amplitude compensation is analyzed below.

Figs. 5–8 are the BP imaging results for multiple targets and Fig. 5 is the image without any amplitude compensation. Figs. 6–8 are the images with propagation loss compensation for the electromagnetic waves, loss adsorption of the refraction waves, and diffusion losses of the spherical wave, respectively, and Fig. 9 shows the result of amplitude compensation for all losses. The panels (a), (b), and (c) of Figs. 5–9 correspond to 2D imaging results, the azimuth-normalized amplitude distribution map, and the range-normalized amplitude distribution map, respectively.

In the panel (a) of Figs. 5–9, the gray part is the wall and the boxes are metal targets. The coordinates of the maximum values of the two targets are (0.65 m, 1.0 9m) and (1.65 m, 1.89 m). When imaging with amplitude compensation for all losses, the coordinates of the post-target are (1.65 m, 1.93 m), 0.04 m behind the front ones. The error is acceptable. Thus, in whatever condition, multiple targets are located at their true positons. In the panels (b) and (c) of Figs. 5–9, the resolution of the azimuth and

range is very high according to the beam width and defocusing phenomena do not exist. The normalized amplitude value will change with different loss compensations. Table 1 gives the actual values. From Table 1, we know that diffusion loss compensation of the spherical wave is highest, absorption loss compensation is second, and propagation loss compensation is minimal. Diffusion loss compensation of a spherical wave plays a leading role. If all losses are compensated, the amplitude value of the pre- and post-target is almost consistent. Thus, loss compensation is very useful for enhancing the scattering intensity of the targets, especially the post-target, and the undetected probability is greatly decreased.

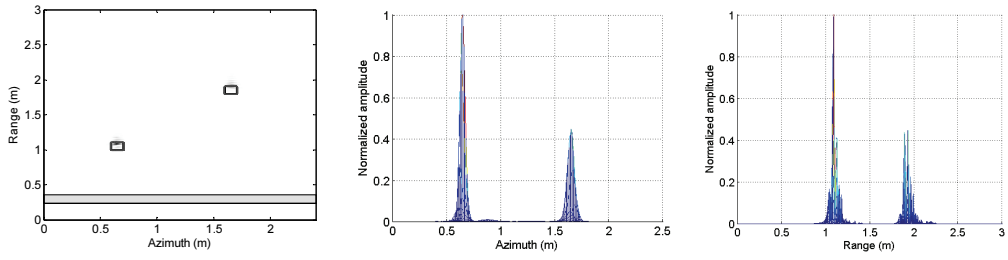

(a) (b) (c)

Fig. 5. Imaging results of a single-layer wall without any amplitude compensation: (a) back projection imaging result, (b) azimuth-normalized amplitude distribution, and (c) range-normalized amplitude distribution.

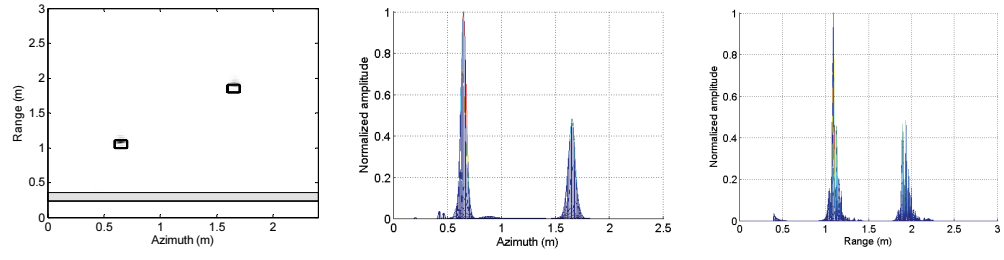

(a) (b) (c)

Fig. 6. Imaging results of a single-layer wall with amplitude compensation of the propagation loss: (a) back projection imaging result, (b) azimuth-normalized amplitude distribution, and (c) Range-normalized amplitude distribution.

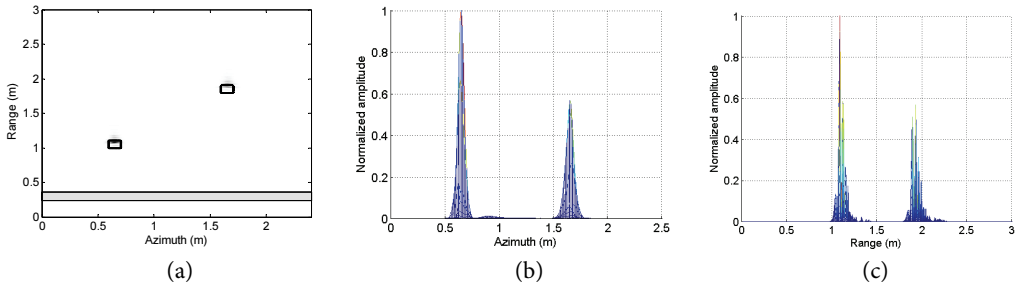

(a) (b) (c)

Fig. 7. Imaging results of a single-layer wall with amplitude compensation of the absorbing loss: (a) back projection imaging result, (b) azimuth-normalized amplitude distribution, and (c) range-normalized amplitude distribution.

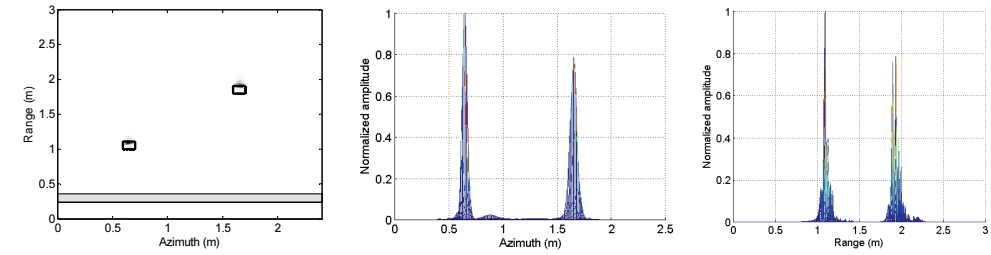

(a) (b) (c)

Fig. 8. Imaging results of a single-layer wall with amplitude compensation of the diffusion loss of spherical wave: (a) back projection imaging result, (b) azimuth-normalized amplitude distribution, and (c) range-normalized amplitude distribution.

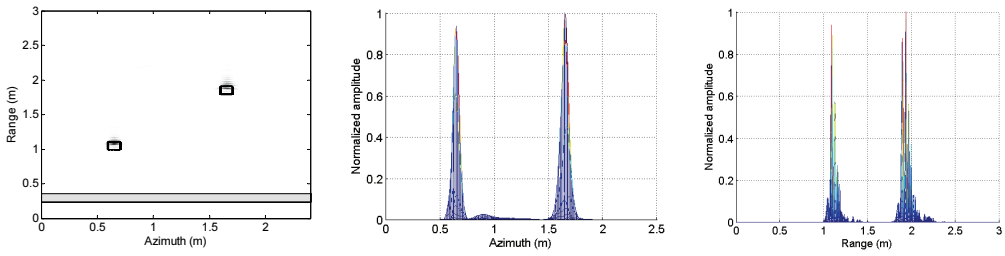

(a) (b) (c)

Fig. 9. Imaging results of a single-layer wall with amplitude compensation for all losses: (a) back projection imaging result, (b) azimuth-normalized amplitude distribution, and (c) range-normalized amplitude distribution.

Next, we considered two-layer walls. Based on the single-layer wall model, a wall with a thickness of 0.05 m was added beneath the original wall and its electromagnetic parameters $(\varepsilon_w^{'}, \mu_w^{'}, \sigma_w^{'})$ were $\varepsilon_w^{'} = 2.6\varepsilon_0, \mu_w^{'} = \mu_0, \sigma_w^{'} = 0.005$. Other conditions were not changed. Because it is time consuming to determine the refraction points at each interface to compensate for every loss in a two-layer wall the sampling interval increased to 0.1 m, and sampling points reduced to 21 under the condition of not influencing imaging quality. Moreover, the diffusion loss of a spherical wave, which is the most important according to forward analysis, was compensated, which is helpful for increasing the scattering intensity of the post-target and greatly reducing the imaging time.

Table 1. Normalized amplitude values of pre- and post-targets under different compensated conditions

	A single-layer wall		Two-layer walls	
	Pre-target	**Post-target**	**Pre-target**	**Post-target**
No compensation	1	0.4387	1	0.3623
Diffusion loss compensation of spherical wave	1	0.7622	1	0.5926
Propagation loss compensation	1	0.4559	NA	
Absorption loss compensation	1	0.5088	NA	
All compensation	0.9367	1	NA	

Fig. 10 shows the imaging results of a two-layer wall with no amplitude compensation. Fig. 11 shows the imaging results of a two-layer wall with an amplitude compensation of diffusion loss for a spherical wave. From Table 2, we know that the maximum amplitude values of the post-target increases greatly

after compensation, but they are still smaller than the maximum amplitude values of the pre-target because only diffusion loss for a spherical wave is compensated, while the other losses are not compensated. In these two cases, the coordinates of the maximum values of the two targets were (0.64 m, 1.09 m) and (1.65 m, 1.89 m), which was consistent with the true center position of the targets. In comparison to the results of the single-layer wall, the imaging quality was a bit poor, and a defocusing phenomenon emerged. This occurred because the sampling points were reduced.

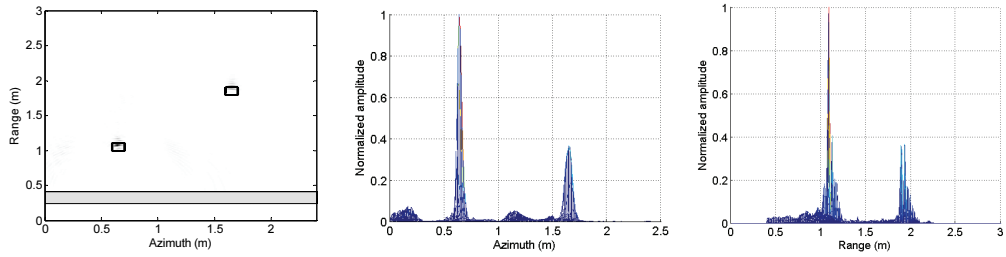

(a) (b) (c)

Fig. 10. Imaging results of two-layer walls with no amplitude compensation. (a) Back projection imaging result, (b) azimuth-normalized amplitude distribution, and (c) range-normalized amplitude distribution.

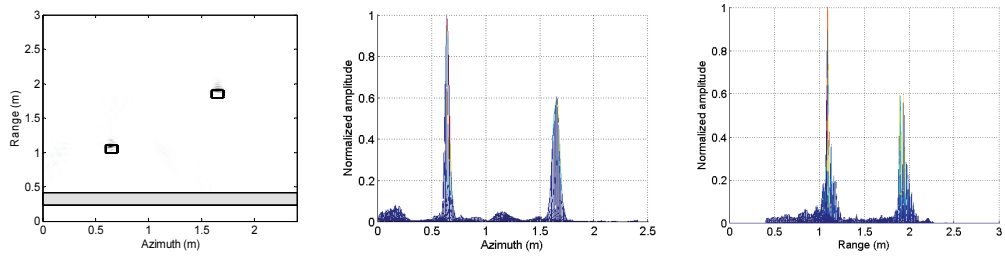

(a) (b) (c)

Fig. 11. Imaging results of two-layer walls with amplitude compensation of diffusion loss for a spherical wave. (a) Back projection imaging result, (b) azimuth-normalized amplitude distribution, and (c) range-normalized amplitude distribution.

Table 2. Calculation time under different compensated conditions (unit: s)

	A single-layer wall	Two-layer walls
No compensation	1,448	53,334
Diffusion loss compensation of spherical wave	1,132	52,583
Propagation loss compensation	2,833	NA
Absorption loss compensation	2,712	NA
All compensation	2,812	NA

Imaging quality must be considered and calculation time is also important. Table 2 gives the calculation time with and without compensation for a single-layer wall and a two-layer wall. The results show that even if the sampling points in a two-layer wall were reduced to a fifth of the amount of a single-layer wall, the calculation time is still 36–46 times larger. If the sampling points in a two-layer wall are the same as the number of those in a single-layer wall, the savings in calculation time are considerable. TWRI requires real-time imaging, and in practice, the wall is made up of multiple layers, so sampling points can be properly reduced under the premise of certain imaging accuracy.

4. Conclusions

A time-delay and amplitude modified BP algorithm is proposed in this paper. The propagation, speed and direction of electromagnetic waves will change through the wall, and the imaging will defocus, smear, and even displace the true position of the target. A time delay was implemented to locate the target in its true position. Loss compensation was primarily discussed, and the propagation loss, absorbing loss, and diffusion loss of a spherical wave were analyzed in detail and compensated in a single wall. Compensation is helpful for enhancing the scattering intensity of the post-target. When all losses are compensated, the scattering intensity of the post-target is almost equal to that of the pre-target. From amongst these items, the diffusion loss compensation of a spherical wave plays a major role, and a two-layer wall model was established. In order to save calculation time, the sampling points were reduced to a fifth of the original, and only the diffusion loss of a spherical wave was compensated. The scattering intensity of the post-target was greatly increased, and the imaging time was dozens of times faster than that of a single-layer wall. High-resolution and focused imaging was obtained in multiple-layer walls with multiple targets.

Acknowledgement

This paper is supported by National Natural Science Foundation of China (Grant No. 61601242), Jiangsu Planned Projects for Postdoctoral Research Funds (No. 1601150C), the Nanjing University of Posts and Telecommunications-Science and Technology Innovation Training Program (NUPT-STITP) (Grant No. XYB2015083) and the Scientific Research Foundation of Nanjing University of Posts and Telecommunications (Grant No. NY215165).

References

[1] H. J. Li and F. L. Lin, "Near-field imaging for conducting objects," *IEEE Transactions on Antennas and Propagation*, vol. 39, no. 5, pp. 600-605, 1999.

[2] W. J. Zhong, C. M. Tong, L. Xin, and G. Yang, "A novel near field imaging approach for through-wall imaging," in *Proceedings of 2011 Cross Strait Quad-Regional Radio Science and Wireless Technology Conference (CSQRWC)*, Harbin, China, 2011, pp. 164-167.

[3] W. J. Zhi, F. Chin, and M. Y. W. Chia, "Near field imaging for breast cancer detection by UWB minimum variance beamforming," in *Proceedings of IEEE International Conference on Ultra-Wideband*, Waltham, MA, 2006, pp. 593-597.

[4] L. Chen and O. Y. Shan, "A time-domain beamformer for UWB through-wall imaging," in *Proceedings of IEEE Region 10 Conference on TENCON*, Taipei, Taiwan, 2007, pp. 1-4.

[5] L. Ma, Z. Z. Zhang, and X. Z. Tan, "Two-step imaging method and resolution analysis for UWB through wall imaging," in *Proceedings of 4th International Conference on Wireless Communications, Networking and Mobile Computing*, Dalian, China, 2008, pp. 1-5.

[6] G. Y. Wang, and M. G. Amin, "Imaging through unknown walls using different standoff distances," *IEEE Transactions on Signal Processing*, vol. 54, no. 10, pp. 4015-4025, 2006.

[7] J. G. Liu, L. J. Kong, X. B. Yang, and Y. Jia, "Imaging auto-focusing with multi-layer non-homogeneous wall in through-wall-radar iamging," in *Proceedings of IEEE Radar Conference*, Atlanta, GA, 2012, pp. 0543-0546.

[8] F. Ahmad, Y. M. Zhang, and M. G. Amin, "three-dimensional wideband beamforming for imaging through a single wall," *IEEE Geoscience and Remote Sensing Letters*, vol. 5, no. 2, pp. 176-179, 2008.

[9] M. Dehmollaian and K. Sarabandi, "Refocusing through building walls using synthetic aperture radar," *IEEE Transactions on Geoscience and Remote Sensing*, vol. 46, no. 6, pp. 1589-1599, 2008.

[10] Y. Jia, L. J. Kong, and X. B. Yang, "Improved cross-correlated back-projection algorithm for through-wall-radar imaging," in *Proceedings of IEEE Radar Conference*, Ottawa, ON, 2013, pp. 1-3.

[11] D. Urdzik, D. Kocur, and J. Rovnakova, "Detection of multiple targets with enhancement of weak UWB radar signals for the purposes of through wall surveillance," in *Proceedings of IEEE 10th International Symposium on Applied Machine Intelligence and Informatics (SAMI)*, Herl'any, Slovakia, 2012, pp. 137-140.

[12] F. Ahmad, M. G. Amin, and S. A. Kassam, "Synthetic aperture beamformer for imaging through a dielectric wall," *IEEE Transactions on Aerospace a d Electronic Systems*, vol. 41, no. 1, pp. 271-283, 2005.

[13] L. Chen and O. Y. Shan, "Through-wall surveillance using ultra-wideband short pulse radar: numerical simulation," in *Proceedings of 2nd IEEE Conference on Industrial Electronics and Applications (ICIEA)*, Harbin, China, 2007, pp. 1551-1554.

[14] W. T. Lei, Y. Su, and C. L. Huang, "A TAM-BP imaging algorithm in GPR application," in *Proceedings of 4th International Conference on Microwave and Millimeter Wave Technology (ICMMT)*, Beijing, China, 2004, pp. 619-621.

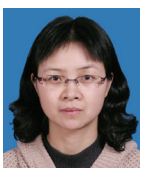

Huamei Zhang http://orcid.org/0000-0002-1608-526X

She received M.S. and Ph.D. degrees in School of Electronic Science and Engineering from Nanjing University of Posts and Telecommunications in 2005 and 2015, respectively. Her current research interests include numerical calculation of electromagnetic field and inverse scattering imaging.

Dongdong Li http://orcid.org/0000-0002-4676-4626

He is with the School of Electronic Science and Engineering from Nanjing University of Posts and Telecommunications as a B.S. candidate since 2013.

Jinlong Zhao http://orcid.org/0000-0002-2924-002X

He is with the School of Electronic Science and Engineering from Nanjing University of Posts and Telecommunications as a B.S. candidate since 2013.

Haitao Wang http://orcid.org/0000-0001-5454-6912

He is with the School of Electronic Science and Engineering from Nanjing University of Posts and Telecommunications as a B.S. candidate since 2013.